Effective Combination Immunotherapy using Oncolytic Viruses to Deliver CAR Targets to Solid Tumors

Anthony K. Park[1,2,3], **Yuman Fong**[3,5], **Sang-In Kim**[3], **Jason Yang**[1], **John P. Murad**[1,2], **Jianming Lu**[3], **Brook Jeang**[1], **Wen-Chung Chang**[1], **Nanhai G. Chen**[3], **Sandra H. Thomas**[5], **Stephen J. Forman**[1,4,6], **Saul J. Priceman**[1,4,6,*]

[1]Department of Hematology and Hematopoietic Cell Transplantation, City of Hope, Duarte, CA 91010, USA

[2]Irell and Manella Graduate School of Biological Sciences, City of Hope, Duarte, CA 91010, USA

[3]Department of Surgery, City of Hope, Duarte, CA 91010, USA

[4]Department of Immuno-Oncology, Beckman Research Institute of City of Hope, Duarte, CA 91010, USA

[5]Department of Clinical and Translational Project Development, City of Hope, Duarte, CA 91010, USA

[6]Co-senior authors

Abstract

Chimeric antigen receptor (CAR)-engineered T cell therapy for solid tumors is limited by the lack of both tumor-restricted and homogeneously expressed tumor antigens. Therefore, we engineered an oncolytic virus to express a non-signaling, truncated CD19 (CD19t) protein for tumor-selective delivery, enabling targeting by CD19-CAR T cells. Infecting tumor cells with an oncolytic vaccinia virus coding for CD19t (OV19t) produced de novo CD19 at the cell surface prior to virus-mediated tumor lysis. Co-cultured CD19-CAR T cells secreted cytokines and exhibited potent cytolytic activity against infected tumors. Using several mouse tumor models, delivery of OV19t promoted tumor control following CD19-CAR T cell administration. Importantly, OV19t induced local immunity characterized by tumor infiltration of endogenous and adoptively-transferred T cells. CAR T cell–mediated tumor killing also induced release of virus from dying tumor cells, which propagated tumor expression of CD19t. Our study features a combination immunotherapy approach using oncolytic viruses to promote de novo CAR T cell targeting of solid tumors.

Introduction:

A major challenge for chimeric antigen receptor (CAR) T cell therapy is the identification of antigens that are truly confined to tumors. In the absence of such restricted expression, CAR T cell therapy poses considerable safety concerns and potentially narrows the therapeutic window for their application against solid tumors[1–3]. CD19 has been an ideal target for CAR T cells against hematological malignancies for several reasons, including its highly restricted expression on B cells and acceptable off-tumor and on-target properties[4]. Extensive studies using CD19-directed CAR T cells have resulted in FDA approvals of CAR T therapies for patients with B-cell malignancies[5,6]. In addition to the shared expression of solid tumor antigens on normal tissue, most of these antigens also have heterogeneous and non-uniform expression patterns in tumors, limiting the potential for effective and durable anti-tumor responses[3,7]. Many solid tumors, including triple-negative breast cancers and liver cancers, lack amenable tumor antigens for CAR T cell development[8]. Therefore, novel approaches to introduce validated targets to tumor cells could potentially broaden the applicability of CAR T cell therapy for otherwise intractable solid tumors.

Oncolytic viruses (OV) are a promising treatment modality for solid tumors. These engineered viruses exhibit tumor selectivity, desirable immunogenic properties, and targeted transgene delivery to tumors[9]. OV have gained momentum in recent years due to their immune-stimulating effects both systemically and in the local tumor microenvironment. The first clinically approved OV, Talimogene laherparepvec (TVEC), is a genetically modified type I herpes simplex virus that expresses granulocyte-macrophage colony-stimulating factor (GM-CSF)[10]. In addition to, and in some respects a consequence of, the selective tumor cell replication of OV and direct tumor cell lysis, TVEC initiates exposure of soluble tumor antigens and induction of host anti-tumor immunity. Combination approaches have exploited OV to bolster the effectiveness of adoptive cellular immunotherapy and immune checkpoint inhibitors[11]. Additionally, versions of OV have been genetically engineered to express cytokines to further improve tumor recruitment of T cells and efficacy of immune checkpoint inhibitors, thereby enhancing overall anti-tumor immunity[12].

Here, we exploited the transgene delivery potential of OV to selectively infect and drive tumor-specific expression of a proof-of-concept CAR-targetable tumor antigen, a truncated non-signaling variant of CD19 (CD19t). The parent version of the chimeric poxvirus-based OV used herein has shown safety and anti-tumor activity in several preclinical models[13–17]. We demonstrated robust cell surface CD19t expression on multiple tumor types infected with OV carrying the CD19t-encoding gene (OV19t), which promoted activation and tumor killing by CD19-specific CAR T cells. Using human tumor xenograft models, as well as immunocompetent mouse tumor models, we showed effective anti-tumor responses by combined treatment with OV19t and CD19-CAR T cells. Importantly, OV19t promoted endogenous T cell, as well as CAR T cell, infiltration into tumors. CD19-CAR T cells also induced the release of intact virus from dying tumor cells, a mechanism by which the combination therapy produced effective tumor regression.

Results

OV effectively delivers CD19t to solid tumor cells in vitro

For these studies, we utilized a oncolytic chimeric orthopoxvirus, designed to infect a large spectrum of tumors[13–17], carrying *CD19t* under the control of the vaccinia synthetic early promoter (P_{SE}) (Fig. 1A). This construction enables rapid expression of *CD19t* and appearance of the protein at the cell surface prior to oncolytic viral-mediated tumor lysis. The human *CD19t* (*hCD19t*) expression cassette was inserted into the *J2R* locus encoding thymidine kinase (*tk*). This modified OV is termed CF33-(SE)hCD19t (hereafter, referred to as OV19t). The inserted *hCD19t* gene replacing *tk* did not significantly impact in vitro infection efficiency or killing activity against human tumor cells (fig. S1, A and B).

To assess the ability of the OV to infect and generate CD19t at the cell surface of tumor cells, we infected the human triple-negative breast cancer cell line, MDA-MB-468, with OV19t for 16 h at varying multiplicity of infection (MOI), and stained tumor cells to detect expression of intracellular vaccinia virus and cell surface CD19t. We observed intracellular OV19t and CD19t at the cell surface in an MOI-dependent manner (Fig. 1B). As a positive control, we compared the OV19t-exposed cells to MDA-MB-468 cells stably expressing CD19t. The intensity of CD19t staining following OV19t exposure appeared higher than with MDA-MB-468 cells that were lentivirally transduced to stably express CD19t under a constitutive *EF1α* promoter (Fig. 1B). We evaluated the percent of tumor cells positive for CD19t after 24 h exposure to varying OV19t MOIs (0.00625 – 1). Flow cytometry showed a MOI-dependent increase in the percent of tumor cells positive for CD19t and vaccinia (Fig. 1C). We observed nearly 100% CD19t positivity of tumors cells after 24 h at an MOI 1 and after 72 h at the lower MOIs (Fig. 1D). With greater than 50% of tumor cells viable at 72 h at these lower MOIs (Fig. 1D, right), we identified a window of opportunity for targeting by CD19-specific CAR T cells. Similar trends of infection efficiency (vaccinia positivity), CD19 positivity, and OV-mediated killing of tumor cells were observed across multiple tumor types, including pancreatic cancer (Capan-1 and Panc-1), prostate cancer (DU145), ovarian cancer (OV90), head and neck cancer (UM-SCC-1 and UM-SCC-47), and glioma (U251T) (Fig. 1E).

OV delivery of CD19t to solid tumor cells redirect activity and cytotoxicity of CD19-CAR T cells in vitro

We assessed whether hCD19t delivered to tumor cells by OV activated CD19-CAR T cells. Tumor cells were infected with OV19t at varying MOIs and cocultured with CD19-CAR T cells at effector:target (E:T) ratios of 1:1 or 1:2 for 24 h. The presence of CD25 and 4–1BB (CD137) were used as cell surface markers of T cell activation and were quantified by flow cytometry. At 24 h, CD19-CAR T cells became activated by OV19t-infected MDA-MB-468 cells in an MOI-dependent manner (fig. S2, A and B). CD19-CAR T cells were also activated by OV19t-infected MDA-MB-231BR (brain-seeking human triple-negative breast cancer) cells after 24 h with similar MOI dependency as seen with MDA-MB-468 cells (fig. S3A). CD19-CAR T cell function was then evaluated by measuring intracellular interferon γ (IFNγ) and cell-surface CD107a by flow cytometry. CD19-CAR T cells cocultured for 16 h

with MDA-MB-468 cells infected with OV19t showed robust activity that depended on the OV19t MOI (Fig. 2A).

To quantify the CD19-CAR T cell activity against tumor cells infected with OV19t, supernatants from cocultures of CD19-CAR T cell and tumor cells infected with OV19t at varying MOI were collected to evaluate CAR-dependent cytokine production. At 24 h, IFNγ secretion was only observed at an MOI of 1. However, at 48 h, IFNγ secretion was detected in an MOI-dependent manner, reaching concentrations nearly equivalent to CD19-CAR T cells cocultured with the positive control, MDA-MB-468 lentivirally transduced to stably express CD19t (Fig. 2B). Interleukin-2 (IL-2) secretion was detected at MOI less than 0.1 at 24 h of coculture and at 48 h was close to the amount produced by the cells cultured with the positive control tumor cells (Fig. 2C).

To evaluate whether CD19-CAR T cell activity leads to killing of OV19t-infected tumor cells, we performed tumor killing assays with MDA-MB-468 and U251T cells. When compared with OV19t-infected tumor cells alone, phase-contrast microscopic analysis of a 72 h time course revealed greater killing of tumor cells infected with OV19t (MOI 0.05) and cocultured with CD19-CAR T cells at all time points (Fig. 2, D and E). We quantified CD19-CAR T cell killing ability against MDA-MB-468 cells (viable CD45-negative) using flow cytometry. At 24 h, we observed greater killing of tumor cells infected with OV19t and cocultured with CD19-CAR T cells than of tumor cells only infected with OV19t (Fig. 2F). At 48 and 72 h, the lowest MOI (0.00625) of OV19t alone induced suboptimal virus-mediated lysis of tumor cells (0 – 20%), whereas the combination of OV19t with CD19-CAR T cells showed greater tumor cell killing (60 – 70%). Similar combination effects were observed with MDA-MB-231BR cells (fig. S3B). Consistent with the loss of viable tumor cells, we found a dramatic reduction in CD19t-positive tumor cells in the combination group at all time points and MOIs evaluated (Fig. 2G). Comparable trends in the reduction of CD19t-positive tumor cells were observed for U251T, OV90, and UM-SCC-47 cells exposed to the combination of OV19t and CD19-CAR T cells (fig. S4). We observed no positive CD19t tumor cells or enhancement of cell killing by CAR T cells when tumor cells were infected with OV-*tk* lacking CD19t (fig. S5, A and B). Taken together, our data suggest that OV are capable of delivering an antigen to tumors, in this case CD19t, and inducing antigen-specific CAR T cell-mediated anti-tumor activity.

Anti-tumor efficacy of combination therapy of OV19t and CD19-CAR T cells in human tumor xenograft models

To first evaluate the anti-tumor activity of OV19t and the dynamics of CD19t induction in infected tumors, we treated mice bearing subcutaneous (s.c.) MDA-MB-468 tumors with a single intratumoral (i.t.) injection of OV19t. We used varying doses [10^5, 10^6, 10^7 plaque forming units (pfu) per mouse] to determine infection efficiency and CD19t positivity in tumors at 3, 7, and 10 d after injection of OV19t (Fig. 3A and fig S6). We determined that 10^7 pfu of OV19t per mouse was optimal for testing combination therapy with CD19-CAR T cells. With 10^7 pfu of OV19t, on day 10 after OV19t injection ~70% of tumor cells were positive for CD19t, which was similar to the values for the positive control of tumors from cells stably expressing CD19t.

We then performed the combination therapy of i.t. delivery of OV19t at 10^7 pfu per mouse, followed 10 d later by i.t. delivery of 5×10^6 of either Mock (untransduced) T cells or CD19-CAR T cells (Fig. 3B). As expected, MDA-MB-468-bearing mice treated with only Mock T cells or CD19-CAR T cells showed no anti-tumor activity. Mice treated with OV19t alone or OV19t in combination with Mock T cells slowed tumor growth. The combination of OV19t and CD19-CAR T cells resulted in marked tumor regression (Fig. 3, B and C). Similar findings were observed when we lowered the OV19t dose by 100-fold to 10^5 pfu (Fig. 3, D). We also confirmed the therapeutic benefits of this combination approach using U251T glioma tumor-bearing mice (Fig. 3, E).

Anti-tumor efficacy of combination therapy of OVm19t and CD19-CAR T cells in a murine immunocompetent tumor model

We next evaluated the therapeutic benefits of this combination approach in an immunocompetent mouse tumor model. We generated OV19t with the murine CD19t gene (OVm19t) and used murine splenic T cells to engineer murine CD19-CAR (mCD19-CAR) T cells. The mCD19-CAR was generated with a retrovirus containing the anti-mouse CD19 single-chain variable fragment (scFv) antigen-binding domain derived from the 1D3 hybridoma as previously described[18], a murine CD8 hinge extracellular spacer and transmembrane domain, a 4–1BB intracellular signaling domain, and a CD3 zeta intracellular signaling domain (fig. S7A). A truncated human epidermal growth factor receptor (hEGFRt) for cell tracking was separated from the CAR with a T2A skip sequence. mCD19-CAR was efficiently transduced in murine splenic T cells (fig. S7B), and mCD19-CAR T cells killed MC38 cells lentivirally engineered to express murine CD19t (fig. S7C).

To evaluate whether mCD19-CAR T cells kill OVm19t-infected MC38 cells, we performed cell killing assays with cocultured cells and quantified killing ability by flow cytometry. We observed greater killing of tumor cells infected with OVm19t and cocultured with mCD19-CAR T cells at 24 h compared with killing of cells infected with OVmCD19t alone (Fig. 4A, left). We detected cells positive for intracellular vaccinia as well as cells positive for cell surface CD19t in an MOI-dependent manner (Fig. 4A, middle and right). CAR T cell-selective tumor killing was highlighted by a reduction in CD19t-positive and OVm19t-positive tumor cells in the combination group at all MOIs evaluated (Fig. 4A, middle and right). These data suggest a combination anti-tumor effect of OV carrying CD19t and mCD19-CAR T cells could be achieved using a fully murine system.

The anti-tumor activity of this combination approach was tested in a syngeneic tumor model using C57BL/6j mice bearing subcutaneous MC38 tumors (Fig. 4B, left). Whereas two doses of 5×10^7 pfu OVm19t injected i.t. every other day produced complete regression and a curative response in only 22% of treated mice, complete regression was achieved in ~60% of mice treated with i.t. OVm19t and i.t. mCD19-CAR T cells (Fig. 4B, right). The therapeutic activity depended on CD19-CAR T cells and OVm19t, because controls with a non-CD19-targeting CAR (mPSCA-CAR) T cell and OV lacking the mCD19t gene (OV-*tk*) failed to show similar anti-tumor activity (fig. S8). We assessed whether intratumoral delivery of OVm19t resulted in infection of non-tumor tissues. Few or no OVm19t infected cells or mCD19t-positive cells were detected in spleen, liver, lung, or ovary from mice

injected intratumorally with OVm19t alone or in combination with mCD19-CAR T cells (fig. S9). These data indicate that off-target effects are minimal with this combination therapy in this model.

We next evaluated the anti-tumor effects of this combination approach using an MC38 peritoneal metastasis model that uses cells expressing firefly luciferase for noninvasive image tracking of the tumors. We found a reduction of tumor burden in (Fig. 4, C and D) and improved overall survival (Fig. 4E) of mice treated with intraperitoneal (i.p.) delivery of both Ovm19t and mCD19-CAR T cells. Considering these results and those from the human xenograft tumor models, we showed the broad applicability of our combination immunotherapy approach with OV-mediated delivery of CD19t antigen and CD19-CAR T cells.

CD19-CAR T cell-mediated tumor killing promotes the release of OV19t

One of the potential pitfalls of using OV to deliver CAR T cell target antigens to tumor cells is the potential for suboptimal or non-uniform infection of solid tumors[19,20]. To address this, we evaluated the effects of mCD19-CAR T cells on the presence of OVm19t in subcutaneous MC38 tumors. Surprisingly, we observed greater apparent spread of OVm19t in the tumor following mCD19-CAR T cell treatment (Fig. 5A). Increased OVm19t infection and percent of cells positive for mCD19t in tumors treated with mCD19-CAR T cells was confirmed in cells isolated from the tumors and analyzed by flow cytometry (Fig. 5B). Using cultured cells, we assessed whether CAR T cell-mediated killing of virally-infected tumor cells enhances the release of oncolytic virus particles for subsequent infection of surrounding tumor cells. MDA-MB-468 tumor cells were first infected with varying MOI of OV19t and then incubated with Mock T cells or CD19-CAR T cells. The supernatants were collected and added to newly plated tumor cells that had not been exposed to either T cells or OV19t (Fig. 5C). The supernatants collected from tumor cells exposed to both OV19t and CD19-CAR T cells resulted in increased infection of naïve tumor cells (Fig. 5, D and E), which resulted in significantly greater tumor cell killing activity (Fig. 5, F and G). The release of oncolytic viral particles from tumor cells dying as a result of antigen-specific CD19-CAR T cell cytotoxicity suggested a mechanism for the more homogeneous OV infection of tumor cells that we observed with this combination immunotherapy approach (Fig. 5A).

OV19t induces endogenous anti-tumor immunity and promotes tumor infiltration of CAR T cells

OV has gained attention for its ability to induce endogenous anti-tumor immunity and recruit T cells to tumors[9]. We therefore assessed the infiltration of T cells into the tumor following OVm19t alone and in combination with mCD19-CAR T cells in the subcutaneous MC38 tumor model. OVm19t induced recruitment of CD3^{+}CD8^{+} cytotoxic T cells to tumors, and this response was amplified in most tumors following the combination of OVm19t and mCD19-CAR T cells (Fig. 6, A and B).

We also evaluated the impact of OVm19t on the recruitment of adoptively-transferred mCD19-CAR T cells expressing firefly luciferase and tracking CAR T cell biodistribution

with noninvasive optical imaging. After i.v. injection of the CAR T cells in mice with MC38 tumors, we observed that mCD19-CAR T cells infiltrated tumors at day 2 after infusion, and this response was enhanced when infused following OVm19t treatment (Fig. 6, C and D). To investigate the development of tumor-specific immune memory in response to the combination therapy, we rechallenged cured mice from Fig. 4B by subcutaneously injecting MC38 cells into the opposite flank from the one containing the cured tumor. Tumors grew with predictable kinetics in treatment-naïve mice but failed to grow in mice previously cured by the combination of OVm19t and mCD19-CAR T cells (Fig. 6E). Taken together, these data indicate that OV19t promoted endogenous anti-tumor immunity as well as tumor recruitment of CD19-CAR T cells.

Discussion

Our findings address two major challenges facing CAR T cell therapies for solid tumors — targeting surface proteins that are heterogeneously distributed in tumors and the presence of these surface proteins on some normal tissues. Here, we demonstrated the capability of OV to deliver a CAR-targetable tumor antigen to solid tumors, using both local tumor and regional metastasis models. We propose that this antigen-delivery method can be clinically translated for solid tumor types that lack amenable tumor antigens for safe and effective targeting by CD19-CAR T cells. CAR T cell therapy and oncolytic virotherapy are complementary modalities for cancer treatment with remarkable potential[21]. Although the introduction of de novo tumor targets distinguishes our approach from other studies combining OV with CAR T cells[22,23], we plan to further modify these OV to express checkpoint pathway inhibitors, cytokines, and chemokines to augment CAR T cell trafficking to tumors and their anti-tumor activities. An important consideration is whether to utilize early, intermediate, or late viral promoters for driving transgene expression. Here, we used an early promoter to drive *CD19t* expression; however, it is worthwhile to evaluate different viral promoters, because this has impacted tumor selectivity and overall therapeutic responses of OV, in particular vaccinia virus[24,25].

Although we performed these proof-of-concept studies using CD19t as a target, this approach has the potential to introduce other targets, including non-human species-specific antigens[26], which may also further enhance the anti-tumor efficacy by eliciting host immunity to foreign proteins. However, targeting of CD19 with CAR T cells is a clinically-validated approach for treating hematological malignancies and has demonstrated clinically-manageable B-cell aplasia[5,6], supporting the future clinical development of this potentially safe and effective combination strategy. Importantly, the combination of OV19t with CD19-CAR T cells resulted in greater viral spread, which can propagate more uniform and widespread distribution of CD19 in the tumor. Also, limited persistence of vaccinia viruses is in part due to antibody-mediated clearance of virus particles[27], which may be dampened by depleting systemic B cells with CD19-CAR T cells, thus improving persistence of OV19t. Future studies are warranted to assess whether B cell depletion with systemically administered CD19-CAR T cells or other modalities improves OV persistence in the combination immunotherapy.

Currently, the only FDA-approved OV, HSV-1-based T-VEC, is delivered by local intratumoral delivery for patients with advanced melanoma. However, the field has been excited about the potential utility of regional or systemic delivery of OV in treating metastatic disease. Most OV clinical and preclinical investigations have evaluated local intratumoral delivery, which has widely demonstrated safety, with local and systemic anti-tumor responses reported in certain cases[28,29]. However, vaccinia-based OV may be well suited for regional or systemic delivery, based on its rapid spread into tissues and its tumor selectivity, which is based on multiple mechanisms including dependence on the EGFR signaling pathway for replication[30,31]. The first clinical report of intravenous delivery of an oncolytic vaccinia virus showed tumor selectivity and was safe in patients[32], which was further supported in follow-up clinical investigations[33]. Recently, the ability to deliver OV regionally to tumors, including intraperitoneally for peritoneal disease, has sparked considerable attention[34–37]. Preclinical studies have suggested robust anti-tumor responses in peritoneal disease models using regional, compared with systemic, delivery of OV[38]. In this study, we evaluated both local intratumoral delivery of OV in a solid tumor model, as well as regional delivery of OV in a peritoneal metastasis model. The regional mode of delivery for this combination therapy is particularly intriguing, because we and others have demonstrated the superiority of regional delivery of CAR T cells in treating peritoneal disease[39–41]. Nonetheless, future investigations are warranted to determine the feasibility and efficacy of systemic delivery of this combination approach with OV and CAR T cells for metastatic disease.

Host immunity is important to the outcome of certain OV, as has been shown for HSV[42]. Additionally, T and natural killer (NK) cells have been identified as major components of host immunity after vaccinia infection and contribute to OV-mediated anti-tumor effects[43], likely due in part to new tumor antigens released from dying tumor cells. Our studies showed OV19t-mediated tumor infiltration of endogenous T cells and CAR T cells, which we hypothesize contribute to a wave of anti-tumor immunity stimulated by the combination therapy. Indeed, we showed tumor-specific immune memory in cured mice that were protected from subsequent tumor rechallenge. We envision that other oncolytic viruses besides vaccinia (for example, HSV, Maraba virus, and adenoviruses) can also be exploited in this combination strategy and that the immunogenic aspects of the therapy may vary depending on the virus.

In addition to the usage of an early promoter, there are several other potential limitations to this study that may impact the translation of anti-tumor efficacy in patients. Although we did not observe cytokine release syndrome or neurotoxicity using CD19-CAR T cells in combination with our oncolytic virus in our mouse models, we cannot rule out this phenomenon in humans, as it has been reported in previous clinical studies[44–46]. Another potential limitation is that our oncolytic virus may infect normal cells leading to unwanted expression of CD19t. While we demonstrated minimal vaccinia or mCD19t expression in normal tissues following intratumoral delivery of OVm19t, sequential administration of the oncolytic virus followed by CD19-CAR T cells may allow normal cells to abort infection and replication, thus favoring tumor-selective expression of CD19t. Furthermore, CD19-CAR T cells may target normal B cells, but the safety of B cell aplasia has been reported when treating patients with hematological malignancies[47,48]. Additionally, immunogenicity

against vaccinia virus may limit the opportunity for repeat injections of OV19t. However, this can potentially be controlled in part by CD19-CAR T cell-mediated elimination of B cells, which may diminish the presence of anti-viral antibodies thereby further facilitating the persistence and activity of this therapeutic combination. Also, previous studies have suggested that extracellular enveloped virus (EEV)-enriched strains can be used to reduce clearance by neutralizing antibodies to possibly allow for systemic delivery of the virus[49]. While we cured over 50% of mice treated with this combination therapy, some mice either responded transiently or did not respond. This can be in part due to heterogeneity of OV-mediated CD19t expression or to checkpoint pathway-mediated resistance, and both CAR T cells and OV have demonstrated induction of PD-L1. This mode of resistance may offer a future opportunity to combine our therapy with immune checkpoint blockade.

In summary, we demonstrated that OV can effectively deliver the CD19-CAR target to solid tumors, which are then susceptible to CD19-CAR T cell-mediated tumor destruction (fig. S10). These findings potentially extend the use of clinically-approved CD19-CAR T cells beyond B-cell malignancies and into a treatment paradigm for multiple solid tumors. Our results specifically inspire further investigations of OV19t, or similar viruses delivering CAR targets, in combination with CAR T cells for the treatment of intractable solid tumors.

Materials and Methods

Study design

In this study, we evaluated a combination approach using oncolytic viruses to induce *de novo* cell surface expression of a truncated nonsignaling version of the CAR target CD19 (CD19t) on solid tumors for subsequent targeting by CD19-CAR T cells. An oncolytic vaccinia virus carrying CD19t (OV19t) was developed to test in combination with CD19-CAR T cells in human solid tumor xenograft models. Murine OV19t (OVm19t) and murine CD19-CAR T cells were developed to test this combination therapy in syngeneic solid tumor mouse models. All in vitro assays were performed with at least duplicate samples, and were repeated in at least 3 independent experiments. *In vivo* studies were performed using 6- to 8-week-old NSG or C57BL/6 mice, using at least three mice per group for all *in vivo* studies, and four to nine mice were included within each group for all therapy and survival studies to ensure statistical power. Prior to OV19t treatment, mice were randomized on the basis of tumor volume or bioluminescent imaging to ensure evenly distributed average tumor sizes across each group. *In vivo* experiments were repeated at least twice. For subcutaneous tumor models, survival was based on the maximum tumor size allowed (approximately 15 mm in diameter). The health condition of mice was monitored daily by the Department of Comparative Medicine at City of Hope, with euthanasia applied according to the American Veterinary Medical Association Guidelines. Investigators were not blinded when monitoring mouse survival. All studies were performed under approved protocols of the Institutional Animal Care and Use Committee (IACUC) and institutional review board (IRB).

Cell lines and viruses

Human triple-negative breast cancer cell line MDA-MB-468 (ATCC HTB-132) was cultured in Dulbecco's Modified Eagle Medium (DMEM) containing 10% fetal bovine

serum (FBS, Hyclone) and 1x antibiotic antimycotic (AA, Gibco), supplemented with 25 mmol/L HEPES (Irvine Scientific) and 2 mmol/L L-glutamine (Thermo Fisher Scientific) (complete DMEM). The brain-seeking human triple-negative breast cancer cell line MDA-MB-231BR[50] (a kind gift from Dr. Patricia S. Steeg, NIH, Bethesda, MD) was cultured in DMEM/Ham F-12 (F12; 1:1) containing 10% FBS and 1x AA. Human pancreatic cancer cell line Capan-1 (ATCC HTB-79) was cultured in Iscove's Modified Dulbecco's Medium (IMDM) containing 20% FBS and 1x AA. Human pancreatic cancer cell line Panc-1 (ATCC CRL-1469) was cultured in Roswell Park Memorial Institute (RPMI) containing 10% FBS and 1x AA. Human ovarian cancer cell line OV90 (ATCC CRL-11732) was cultured in 1:1 volume of MCDB 105 medium (Sigma-Aldrich) and Medium 199 (Gibco) containing 20% FBS and 1x AA. Human head and neck carcinoma line UM-SCC-1 (EMD Millipore) was cultured in DMEM containing 20% FBS, 1x AA, and 1x non-essential amino acids (NEAA, Life Technologies). Human head and neck carcinoma line UM-SCC-47 (EMD Millipore) was cultured in DMEM containing 10% FBS, 1x AA, and 1x NEAA. Human prostate cancer cell line DU145 (ATCC HTB-81) was cultured in RPMI containing 10% FBS and 1x AA. Human glioblastoma cell line U251T (gift from Dr. Waldemar Debinski, Wake Forest School of Medicine) was cultured in complete DMEM. Human embryonic kidney cell line 293T (ATCC CRL-3216) and human fibrosarcoma cell line HT1080 (ATCC CCL-121) were cultured in complete DMEM. African green monkey kidney fibroblasts (CV-1) (ATCC CCL-70) were cultured in DMEM containing 10% FBS and 1x AA. CV-1 cells were used for both amplification and titration of orthopoxviruses. Murine colon adenocarcinoma cell line MC38 (obtained from the National Institutes of Health) was cultured in complete DMEM.

Generation of recombinant chimeric orthopoxvirus expressing human and murine truncated CD19 (CD19t)

To generate a shuttle vector containing the human (hCD19t) or murine (mCD19t) CD19t expression cassette with the VACV synthetic early (SE) promoter, the hCD19t and mCD19t cDNAs were PCR-amplified from the plasmids hCD19t-2A-IL2-pHIV7 and mCD19t-epHIV7 using Q5 High-Fidelity 2X Master Mix (New England Biolabs Inc., Ipswich, MA) and the primers: 5'-GCG TCG ACC ACC ATG CCA CCT CCT CGC CTC CTC TTC TTC CCT CCT CTT CCTC-3' and 5'-GCG GGA TCC ATA AAA ATT AAT TAA TCA TCT TTT CCT CCT CAG GAC CAG GGC TCT TTG AAG ATG-3'. The PCR fragment was digested with *Sal* I and *Bam*H I and cloned into the same-cut p33NCTK-SE-hNIS replacing hNIS to yield p33NCTK-SE-hCD19t and p33NCTK-SE-mCD19t. The hCD19t and mCD19t cDNAs in p33NCTK-SE-hCD19t and p33NCTK-SE-mCD19t were confirmed by sequencing. CV-1 cells were infected with CF33[16] at an MOI of 0.1 for 1 h and then transfected with p33NCTK- SE-hCD19t and p33NCTK-SE-mCD19t by use of jetPRIME in vitro DNA and siRNA transfection reagent (Polyplus-transfection Inc., New York, NY). Two days after infection, infected and transfected cells were harvested and the recombinant viruses (OV19t) were selected and plaque purified as described previously[51].

DNA constructs

MDA-MB-468 and MDA-MB-231BR cells were engineered to express hCD19t by transduction with epHIV7 lentivirus carrying the human *CD19t* gene under the control of the

EF1a promoter. A similar procedure was used to engineer MC38 cells to express mCD19t. The human CD19–28ζ CAR lentiviral construct with truncated human EGFR (hEGFRt) separated by a T2A ribosome skip sequence was previously described[52]. The murine CD19-BBζ CAR (mCD19-CAR) retroviral construct (pMYs, Cell Biolabs Inc.) contained an anti-mouse CD19-targeted single-chain variable fragment (scFv) sequence derived from the 1D3 hybridoma[18], a murine CD8 hinge extracellular spacer and transmembrane domain, a murine 4–1BB intracellular costimulatory signaling domain, a murine CD3ζ cytolytic domain, and the hEGFRt separated from the CAR by a T2A ribosome skip sequence. A similar CAR construct was used to generate the murine PSCA-BBζ CAR (mPSCA-CAR), which contained an anti-human PSCA-targeted scFv sequence derived from the 1G8 hybridoma[53]. The firefly luciferase (ffluc) gene was cloned into a murine stem cell virus (MSCV, Addgene) retroviral construct.

Human T cell enrichment, lentivirus production and transduction, and ex vivo expansion

T-cell isolation, lentivirus production and transduction, and ex vivo expansion of CAR T cells was performed as previously described[54]. Untransduced (Mock) human T cells in all studies were processed in parallel with CAR T cells.

Murine retrovirus production

Retrovirus was generated by plating PlatE cells for 1 week in complete DMEM with the addition of selection antibiotics: 1 μg/mL puromycin (InvivoGen) and 10 μg/mL blasticidin (InvivoGen). One day prior to production, cells were washed once and cultured with warm antibiotic-free complete DMEM. On the day of transfection, cells were washed again and 6 μg of plasmid DNA was added with FugeneHD transfection reagent (Promega). Supernatants were collected at 24, 36, and 48 h and frozen at −80°C until further use.

Murine T cell enrichment, transduction, and ex vivo expansion

Mouse splenocytes were obtained from naïve C57BL/6j mice (The Jackson Laboratory), and T cells were isolated using the EasySep Mouse T Cell Isolation Kit (StemCell Technologies) according to the manufacturer's protocol. Freshly isolated mouse T cells were cultured in RPMI media containing 10% FBS (Hyclone), 50 U/mL recombinant human IL-2 (Novartis Oncology), 10 ng/mL recombinant murine IL-7 (Peprotech), and 50 μM 2-mercaptoethanol (Gibco). For CAR retroviral transduction, T cells were cultured with mouse CD3/CD28 Dynabeads (Invitrogen) overnight, and plated onto Retronectin (Takara)-coated 24-well non-treated tissue culture plates (Corning Life Sciences) with 1 mL of mCD19-CAR or ffluc retrovirus or both. For mPSCA-CAR T cells used as negative controls, T cells were cultured and plated as described above with 1 mL of mPSCA-CAR retrovirus. Plates were spinoculated at 1500 *g* for 1 h at 32°C. After culturing the transduced cells for 4 days, beads were magnetically removed and T cells were used for in vitro functional assays and in vivo tumor models. Purity and phenotype of CAR T cells were confirmed by flow cytometry.

Intracellular and extracellular staining and flow cytometry

Flow cytometric analysis was performed as previously described[54]. T cell activation was determined by using antibodies against CD25, CD107a, CD137, and IFNγ (BD

Biosciences). Tumor cells were identified using an antibody recognizing Ep-CAM (CD326) (BioLegend). Cell viability was determined using LIVE/DEAD Fixable Violet Dead Cell Stain Kit for 405 nm excitation (Invitrogen). For vaccinia staining, cells were fixed and permeabilized using BD Cytofix/Cytoperm Fixation/Permeabilization Solution Kit according to the manufacturer's protocol (BD Biosciences). Cells were then incubated with anti-vaccinia virus primary antibody (Abcam) and incubated for 30 minutes at 4°C in the dark. The cells were washed twice prior to secondary stain with Goat Anti-Rabbit IgG H&L (Alexa Fluor 488) (Abcam) for 30 minutes at 4°C in the dark. The cells were then washed twice prior to resuspension in FACS buffer and acquisition on the MACSQuant Analyzer 10 (Miltenyi Biotec). Data were analyzed with FlowJo software (v10, TreeStar).

OV transduction and T-cell functional assays

For OV transduction and tumor killing assays, CAR T cells and tumor targets were co-cultured at varying effector T cell to tumor cell ratios along with the addition of varying MOIs of OV19t in complete X-VIVO (Lonza) in the absence of exogenous cytokines in round-bottom 96-well tissue culture-treated plates (Corning) for 1 – 3 days and analyzed by flow cytometry as described above. Tumor cell killing by CAR T cells with or without OV19t was calculated by comparing CD45-negative cell counts relative to that observed by Mock T cells from the same healthy donor. For T cell activation assays, CAR T cells and tumor targets were cocultured at an effector T cell to tumor cell ratios of 1:1 or 1:2 along with the addition of varying MOIs of OV19t in complete X-VIVO in the absence of exogenous cytokines in 96-well plates for 1 – 3 d and analyzed by flow cytometry for specific markers of T cell activation. A similar procedure was followed for mouse functional assays using OVmCD19t, using complete RPMI instead of X-VIVO, and at an effector T cell to tumor cell ratio of 1:1. For degranulation and intracellular cytokine assays, CAR T cells and tumor targets were cocultured at varying effector T cell to tumor cell ratios along with the addition of varying MOIs of OV19t in complete X-VIVO in the absence of exogenous cytokines in round-bottom 96-well plates. Anti-CD107a antibody was added to the cultures for 16 – 18 h at 37°C, cells were then fixed and permeabilized, and stained with anti-IFNγ antibody before analysis by flow cytometry.

Viral Plaque Assay

Following infection of cells with virus as mentioned above, supernatants were collected and processed as previously described[16].

Immunofluorescence Microscopy

Tumor cell lines were analyzed for vaccinia infection and CD19t by immunofluorescence microscopy. MDA-MB-468 or MDA-MB-468-CD19t cells (4×10^4) were plated in individual wells of 96-well glass bottom plates (Cellvis) and incubated for 24 h to allow for cells to adhere. Media was aspirated from each well, and cells were gently washed with PBS (pH 7.4) + 1% bovine serum albumin (BSA). Cells were stained with primary CD19 antibody (Abcam) at 4°C for 1 h, washed, and stained with secondary streptavidin AlexaFluor 647 (Invitrogen) for 1 h at room temperature. Cells were then fixed and permeabilized using Cytofix/Cytoperm Fixation/Permeabilization Solution (BD Biosciences) for 10 min at room temperature. The solution was aspirated and stained with

anti-vaccinia antibody (Abcam) for 1 h at room temperature, washed, and stained with goat anti-rabbit IgG AlexaFluor 488 (Abcam) for 1 h. Cells were stained with 4'6-diamidino-2-phenylindole (DAPI) for 5 minutes at room temperature and each well was imaged at 10 – 63X magnification.

Cytokine ELISA

Tumor cells and CD19-CAR T cells were plated into 96-well round bottom plates (Costar) and varying MOIs of OV19t (OVmCD19t) were added. Following incubations at 37°C for 24, 48, or 72 h, supernatants were collected and analyzed according to the Human or Mouse IFNγ or IL-2 ELISA Ready-SET-GO! (eBioscience) manufacturer's protocol. Plates were read at 450 nm using the Cytation 3 Cell Imaging Multi-Mode Reader and Gen5 Microplate Reader and Imager Software (BioTek).

xCELLigence

The xCELLigence real-time cell analysis (RTCA) instrument (ACEA Biosciences) was used for impedance experiments to determine tumor cell killing according to the manufacturer's protocol. Briefly, tumor cells were plated at 25,000 cells per well and cocultured with varying MOIs of OV19t and incubated at 37°C for 3 h. Fresh media was added to remove any residual viral particles. Next, the cells were incubated for an additional 4 h, and Mock T cells or CAR T cells were added for 18 h. Supernatants were collected, sonicated three times, and added to freshly plated tumor cells to evaluate cell killing.

In vivo tumor studies

All animal experiments were performed under protocols approved by the City of Hope Institutional Animal Care and Use Committee. For human tumor xenograft studies, MDA-MB-468 and MDA-MB-468-CD19t cells (5×10^6 cells/mouse) or U251T cells (1×10^6 cells/mouse) were prepared in Hank's Balanced Salt Solution without Ca^{2+} and Mg^{2+} ($HBSS^{-/-}$) and injected subcutaneously (s.c.) into the flank of female NSG mice. Tumor growth was monitored 2 – 3 times per week by caliper measurement. Once tumor volumes reached approximately 100 – 300 mm^3, OV19t viruses prepared and diluted in PBS (pH 7.4) were intratumorally (i.t.) administered at 10^3 – 10^7 pfu/mouse. For combination therapy studies, CAR T cells (5×10^6 cells/mouse) were prepared in PBS (pH 7.4) and injected i.t. 5 – 10 d after OV treatment. For OV19t transduction studies, mice were euthanized and tumors were harvested and processed for flow cytometry (described above) at 3, 7, or 10 days after OV19t treatment. For all studies, mice were euthanized and tumors were harvested and processed for flow cytometry once tumors reached no more than 15 mm in diameter.

For s.c. immunocompetent mouse studies, MC38 cells (5×10^5 cells/mouse) were prepared in $HBSS^{-/-}$ containing 1:1 v:v of growth-factor reduced Matrigel (Corning Life Sciences) and engrafted in the flank of female C57BL/6j mice by s.c. injection. Tumor growth was monitored 2 – 3 times per week by caliper measurement. Once tumor volumes reached approximately 50 – 150 mm^3, OV19t viruses prepared and diluted in PBS (pH 7.4) were i.t. administered for a total of 2 doses of 10^7 pfu/mouse per dose. For combination therapy studies, mCD19-CAR T cells (5×10^6 cells/mouse) were prepared in PBS and i.t. injected 2

days after the last OV treatment. For the rechallenge studies, mice with complete responses following OVm19t in combination with mCD19-CAR T cells were injected with MC38 cells (5×10^5 cells/mouse) in the opposite flank. Treatment-naïve mice were also included in this study to confirm tumor growth. Tumor growth was monitored 2 – 3 times per week by caliper measurement.

For immunocompetent peritoneal metastasis mouse studies, MC38 cells expressing firefly luciferase (5×10^5 cells/mouse) were prepared in HBSS$^{-/-}$ and engrafted in female C57BL/6j mice by intraperitoneal (i.p.) injection in the lower left quadrant of the abdomen. Tumor growth was monitored at least once a week by non-invasive optical imaging (LagoX) and flux was analyzed with Living Image software (Aura). Mice were imaged following i.p. injection of 150 – 250 μL of D-luciferin potassium salt (Perkin Elmer) suspended in PBS (pH 7.4) (4.29 mg/mouse). On day 6 after tumor injection, OVm19t was prepared in PBS and i.p. administered at 5×10^7 pfu/mouse. For combination therapy studies, mCD19-CAR T cells (5×10^6 cells/mouse) were prepared in PBS and injected i.p. 2 days after the final OV treatment. Moribund mice, (that is pale, hunched, lethargic, and having distended abdomen) as assessed by the on-site animal health technician or veterinarian, were euthanized.

For T-cell tracking studies, s.c. MC38-tumor bearing C57BL/6j mice were injected with i.t. OVm19t alone, intravenous (i.v.) firefly luciferase-expressing mCD19-CAR T cells alone or the combination of i.t. OVm19t and i.v. firefly luciferase-expressing mCD19-CAR T cells. T-cell biodistribution was monitored by non-invasive optical imaging (LagoX) and flux was analyzed with Living Image software (Aura).

Immunohistochemistry

Tumor tissues were harvested and fixed for 48 – 72 hours in 4% paraformaldehyde (4%PFA, Boston BioProducts) and stored in 70% ethanol until further processing. Paraffin-embedded tumor sections (10 μm) were deparaffinized followed by heat-mediated antigen retrieval for 30 minutes in IHC-TEK epitope retrieval solution (IHC World). Following antigen retrieval, tumor sections were permeabilized with 100% methanol. Sections were blocked for 30 minutes with Tris-NaCl (TNB) blocking buffer (PerkinElmer), and then incubated with rabbit anti-vaccinia virus antibody (Abcam) diluted 1:100 in TNB blocking buffer overnight in a humidified chamber at 4°C. Following incubation, tumor sections were wash and incubated with Alexa-Fluor-488-conjgated goat anti-rabbit secondary antibody (Abcam) for 1 hour at room temperature. Finally, the sections were counterstained with DAPI.

Immunohistochemistry for CD3 and CD8 were performed by the Pathology Core at City of Hope. Briefly, deparaffinized tumor sections (10 μm) were stained with hematoxylin & eosin (H&E, Sigma-Aldrich), rat anti-mouse CD3 (Abcam), and rat anti-mouse CD8a (Novus Biologicals). Images were obtained using the Nanozoomer 2.0HT digital slide scanner and the associated NDP.view2 software (Hamamatzu). For CD8 quantification after IHC staining, ImageJ (NIH) analysis was performed as per the standard recommended algorithm[55].

Statistical analysis

Data are presented as mean ± standard deviation (SD), unless otherwise stated. Statistical comparisons between groups were performed using the unpaired two-tailed Student's t-test to calculate p-value, unless otherwise stated. Statistical comparison of Kaplan-Meier survival data was performed using the log-rank (Mantel-Cox) test. Original data are in data file S1.

Supplementary Material

Refer to Web version on PubMed Central for supplementary material.

Acknowledgments:

Data and materials availability:

All data associated with this study are present in the paper or Supplementary Materials. OV19t and CD19-CAR constructs are available from SJP under a material transfer agreement with City of Hope.

References and notes:

1. June CH, O'Connor RS, Kawalekar OU, Ghassemi S. & Milone MC CAR T cell immunotherapy for human cancer. Science 359, 1361–1365, doi:10.1126/science.aar6711 (2018). [PubMed: 29567707]

2. Priceman SJ, Forman SJ & Brown CE Smart CARs engineered for cancer immunotherapy. Curr Opin Oncol 27, 466–474, doi:10.1097/CCO.0000000000000232 (2015). [PubMed: 26352543]

3. Fesnak AD, June CH & Levine BL Engineered T cells: the promise and challenges of cancer immunotherapy. Nature reviews. Cancer 16, 566–581, doi:10.1038/nrc.2016.97 (2016).

4. Davila ML & Sadelain M. Biology and clinical application of CAR T cells for B cell malignancies. Int J Hematol 104, 6–17, doi:10.1007/s12185-016-2039-6 (2016). [PubMed: 27262700]

5. Liu Y, Chen X, Han W. & Zhang Y. Tisagenlecleucel, an approved anti-CD19 chimeric antigen receptor T-cell therapy for the treatment of leukemia. Drugs Today (Barc) 53, 597–608, doi:10.1358/dot.2017.53.11.2725754 (2017). [PubMed: 29451276]

6. Sharma P, King GT, Shinde SS, Purev E. & Jimeno A. Axicabtagene ciloleucel for the treatment of relapsed/refractory B-cell non-Hodgkin's lymphomas. Drugs Today (Barc) 54, 187–198, doi:10.1358/dot.2018.54.3.2776625 (2018). [PubMed: 29771253]

7. O'Rourke DM et al. A single dose of peripherally infused EGFRvIII-directed CAR T cells mediates antigen loss and induces adaptive resistance in patients with recurrent glioblastoma. Science translational medicine 9, doi:10.1126/scitranslmed.aaa0984 (2017).

8. Schmidts A. & Maus MV Making CAR T Cells a Solid Option for Solid Tumors. Frontiers in immunology 9, 2593, doi:10.3389/fimmu.2018.02593 (2018). [PubMed: 30467505]

9. Kaufman HL, Kohlhapp FJ & Zloza A. Oncolytic viruses: a new class of immunotherapy drugs. Nat Rev Drug Discov 14, 642–662, doi:10.1038/nrd4663 (2015). [PubMed: 26323545]

10. Rehman H, Silk AW, Kane MP & Kaufman HL Into the clinic: Talimogene laherparepvec (T-VEC), a first-in-class intratumoral oncolytic viral therapy. J Immunother Cancer 4, 53, doi:10.1186/s40425-016-0158-5 (2016). [PubMed: 27660707]

11. Sivanandam V, LaRocca CJ, Chen NG, Fong Y. & Warner SG Oncolytic Viruses and Immune Checkpoint Inhibition: The Best of Both Worlds. Molecular therapy oncolytics 13, 93–106, doi:10.1016/j.omto.2019.04.003 (2019). [PubMed: 31080879]

12. Bommareddy PK, Shettigar M. & Kaufman HL Integrating oncolytic viruses in combination cancer immunotherapy. Nat Rev Immunol, doi:10.1038/s41577-018-0014-6 (2018).

13. Chaurasiya S. et al. A chimeric poxvirus with J2R (thymidine kinase) deletion shows safety and anti-tumor activity in lung cancer models. Cancer gene therapy, doi:10.1038/s41417-019-0114-x (2019).

14. Warner SG et al. A Novel Chimeric Poxvirus Encoding hNIS Is Tumor-Tropic, Imageable, and Synergistic with Radioiodine to Sustain Colon Cancer Regression. Molecular therapy oncolytics 13, 82–92, doi:10.1016/j.omto.2019.04.001 (2019). [PubMed: 31061881]

15. O'Leary MP et al. A Novel Oncolytic Chimeric Orthopoxvirus Encoding Luciferase Enables Real-Time View of Colorectal Cancer Cell Infection. Molecular therapy oncolytics 9, 13–21, doi:10.1016/j.omto.2018.03.001 (2018). [PubMed: 29988502]

16. Choi AH et al. Endogenous Akt Activity Promotes Virus Entry and Predicts Efficacy of Novel Chimeric Orthopoxvirus in Triple-Negative Breast Cancer. Molecular therapy oncolytics 9, 22–29, doi:10.1016/j.omto.2018.04.001 (2018). [PubMed: 29988465]

17. O'Leary MP et al. Novel oncolytic chimeric orthopoxvirus causes regression of pancreatic cancer xenografts and exhibits abscopal effect at a single low dose. Journal of translational medicine 16, 110, doi:10.1186/s12967-018-1483-x (2018). [PubMed: 29699566]

18. Kochenderfer JN, Yu Z, Frasheri D, Restifo NP & Rosenberg SA Adoptive transfer of syngeneic T cells transduced with a chimeric antigen receptor that recognizes murine CD19 can eradicate lymphoma and normal B cells. Blood 116, 3875–3886, doi:10.1182/blood-2010-01-265041 (2010). [PubMed: 20631379]

19. Martin NT & Bell JC Oncolytic Virus Combination Therapy: Killing One Bird with Two Stones. Mol Ther 26, 1414–1422, doi:10.1016/j.ymthe.2018.04.001 (2018). [PubMed: 29703699]

20. Twumasi-Boateng K, Pettigrew JL, Kwok YYE, Bell JC & Nelson BH Oncolytic viruses as engineering platforms for combination immunotherapy. Nat Rev Cancer 18, 419–432, doi:10.1038/s41568-018-0009-4 (2018). [PubMed: 29695749]

21. Ajina A. & Maher J. Prospects for combined use of oncolytic viruses and CAR T-cells. Journal for immunotherapy of cancer 5, 90, doi:10.1186/s40425-017-0294-6 (2017). [PubMed: 29157300]

22. Wing A. et al. Improving CART-Cell Therapy of Solid Tumors with Oncolytic Virus-Driven Production of a Bispecific T-cell Engager. Cancer immunology research 6, 605–616, doi:10.1158/2326-6066.CIR-17-0314 (2018). [PubMed: 29588319]

23. Nishio N. et al. Armed oncolytic virus enhances immune functions of chimeric antigen receptor-modified T cells in solid tumors. Cancer Res 74, 5195–5205, doi:10.1158/0008-5472.CAN-14-0697 (2014). [PubMed: 25060519]

24. Chen H, Sampath P, Hou W. & Thorne SH Regulating cytokine function enhances safety and activity of genetic cancer therapies. Molecular therapy : the journal of the American Society of Gene Therapy 21, 167–174, doi:10.1038/mt.2012.225 (2013). [PubMed: 23281444]

25. Chen B. et al. Evaluation of cytokine toxicity induced by vaccinia virus-mediated IL-2 and IL-12 antitumour immunotherapy. Cytokine 15, 305–314, doi:10.1006/cyto.2001.0906 (2001). [PubMed: 11594797]

26. Kumaresan PR et al. Bioengineering T cells to target carbohydrate to treat opportunistic fungal infection. Proceedings of the National Academy of Sciences of the United States of America 111, 10660–10665, doi:10.1073/pnas.1312789111 (2014). [PubMed: 25002471]

27. Xu R, Johnson AJ, Liggitt D. & Bevan MJ Cellular and humoral immunity against vaccinia virus infection of mice. Journal of immunology 172, 6265–6271, doi:10.4049/jimmunol.172.10.6265 (2004).

28. Cripe TP et al. Phase 1 study of intratumoral Pexa-Vec (JX-594), an oncolytic and immunotherapeutic vaccinia virus, in pediatric cancer patients. Molecular therapy : journal of

the American Society of Gene Therapy 23, 602–608, doi:10.1038/mt.2014.243 (2015). [PubMed: 25531693]

29. Breitbach CJ, Moon A, Burke J, Hwang TH & Kirn DH A Phase 2, Open-Label, Randomized Study of Pexa-Vec (JX-594) Administered by Intratumoral Injection in Patients with Unresectable Primary Hepatocellular Carcinoma. Methods in molecular biology 1317, 343–357, doi:10.1007/978-1-4939-2727-2_19 (2015). [PubMed: 26072416]

30. Beerli C. et al. Vaccinia virus hijacks EGFR signalling to enhance virus spread through rapid and directed infected cell motility. Nat Microbiol 4, 216–225, doi:10.1038/s41564-018-0288-2 (2019). [PubMed: 30420785]

31. Yang H. et al. Antiviral chemotherapy facilitates control of poxvirus infections through inhibition of cellular signal transduction. The Journal of clinical investigation 115, 379–387, doi:10.1172/JCI23220 (2005). [PubMed: 15690085]

32. Breitbach CJ et al. Intravenous delivery of a multi-mechanistic cancer-targeted oncolytic poxvirus in humans. Nature 477, 99–102, doi:10.1038/nature10358 (2011). [PubMed: 21886163]

33. Downs-Canner S. et al. Phase 1 Study of Intravenous Oncolytic Poxvirus (vvDD) in Patients With Advanced Solid Cancers. Molecular therapy : the journal of the American Society of Gene Therapy 24, 1492–1501, doi:10.1038/mt.2016.101 (2016). [PubMed: 27203445]

34. Hung CF et al. Vaccinia virus preferentially infects and controls human and murine ovarian tumors in mice. Gene therapy 14, 20–29, doi:10.1038/sj.gt.3302840 (2007). [PubMed: 16915291]

35. Coukos G, Courreges MC & Benencia F. Intraperitoneal oncolytic and tumor vaccination therapy with replication-competent recombinant virus: the herpes paradigm. Current gene therapy 3, 113–125, doi:10.2174/1566523034578401 (2003). [PubMed: 12653405]

36. Lauer UM et al. Phase I Study of Oncolytic Vaccinia Virus GL-ONC1 in Patients with Peritoneal Carcinomatosis. Clinical cancer research : an official journal of the American Association for Cancer Research 24, 4388–4398, doi:10.1158/1078-0432.CCR-18-0244 (2018). [PubMed: 29773661]

37. Fountzilas C, Patel S. & Mahalingam D. Review: Oncolytic virotherapy, updates and future directions. Oncotarget 8, 102617–102639, doi:10.18632/oncotarget.18309 (2017). [PubMed: 29254276]

38. Kulu Y. et al. Comparison of intravenous versus intraperitoneal administration of oncolytic herpes simplex virus 1 for peritoneal carcinomatosis in mice. Cancer gene therapy 16, 291–297, doi:10.1038/cgt.2008.83 (2009). [PubMed: 18989355]

39. Murad JP et al. Effective Targeting of TAG72(+) Peritoneal Ovarian Tumors via Regional Delivery of CAR-Engineered T Cells. Frontiers in immunology 9, 2268, doi:10.3389/fimmu.2018.02268 (2018). [PubMed: 30510550]

40. Koneru M, Purdon TJ, Spriggs D, Koneru S. & Brentjens RJ IL-12 secreting tumor-targeted chimeric antigen receptor T cells eradicate ovarian tumors in vivo. Oncoimmunology 4, e994446, doi:10.4161/2162402X.2014.994446 (2015).

41. Chekmasova AA et al. Successful eradication of established peritoneal ovarian tumors in SCID-Beige mice following adoptive transfer of T cells genetically targeted to the MUC16 antigen. Clinical cancer research : an official journal of the American Association for Cancer Research 16, 3594–3606, doi:10.1158/1078-0432.CCR-10-0192 (2010). [PubMed: 20628030]

42. Yin J, Markert JM & Leavenworth JW Modulation of the Intratumoral Immune Landscape by Oncolytic Herpes Simplex Virus Virotherapy. Frontiers in oncology 7, 136, doi:10.3389/fonc.2017.00136 (2017). [PubMed: 28695111]

43. Zamarin D. et al. Localized oncolytic virotherapy overcomes systemic tumor resistance to immune checkpoint blockade immunotherapy. Science translational medicine 6, 226ra232, doi:10.1126/scitranslmed.3008095 (2014).

44. Hay KA et al. Kinetics and biomarkers of severe cytokine release syndrome after CD19 chimeric antigen receptor-modified T-cell therapy. Blood 130, 2295–2306, doi:10.1182/blood-2017-06-793141 (2017). [PubMed: 28924019]

45. Gust J. et al. Endothelial Activation and Blood-Brain Barrier Disruption in Neurotoxicity after Adoptive Immunotherapy with CD19 CAR-T Cells. Cancer discovery 7, 1404–1419, doi:10.1158/2159-8290.CD-17-0698 (2017). [PubMed: 29025771]

46. Davila ML et al. Efficacy and toxicity management of 19–28z CAR T cell therapy in B cell acute lymphoblastic leukemia. Science translational medicine 6, 224ra225, doi:10.1126/scitranslmed.3008226 (2014).

47. Brentjens RJ et al. Safety and persistence of adoptively transferred autologous CD19-targeted T cells in patients with relapsed or chemotherapy refractory B-cell leukemias. Blood 118, 4817–4828, doi:10.1182/blood-2011-04-348540 (2011). [PubMed: 21849486]

48. Maude SL, Teachey DT, Porter DL & Grupp SA CD19-targeted chimeric antigen receptor T-cell therapy for acute lymphoblastic leukemia. Blood 125, 4017–4023, doi:10.1182/blood-2014-12-580068 (2015). [PubMed: 25999455]

49. Kirn DH, Wang Y, Liang W, Contag CH & Thorne SH Enhancing poxvirus oncolytic effects through increased spread and immune evasion. Cancer research 68, 2071–2075, doi:10.1158/0008-5472.CAN-07-6515 (2008). [PubMed: 18381410]

50. Palmieri D. et al. Her-2 overexpression increases the metastatic outgrowth of breast cancer cells in the brain. Cancer research 67, 4190–4198, doi:10.1158/0008-5472.CAN-06-3316 (2007). [PubMed: 17483330]

51. Falkner FG & Moss B. Transient dominant selection of recombinant vaccinia viruses. J Virol 64, 3108–3111 (1990). [PubMed: 2159565]

52. Wang X. et al. Phase 1 studies of central memory-derived CD19 CAR T-cell therapy following autologous HSCT in patients with B-cell NHL. Blood 127, 2980–2990, doi:10.1182/blood-2015-12-686725 (2016). [PubMed: 27118452]

53. Gu Z, Yamashiro J, Kono E. & Reiter RE Anti-prostate stem cell antigen monoclonal antibody 1G8 induces cell death in vitro and inhibits tumor growth in vivo via a Fc-independent mechanism. Cancer research 65, 9495–9500, doi:10.1158/0008-5472.CAN-05-2086 (2005). [PubMed: 16230414]

54. Priceman SJ et al. Co-stimulatory signaling determines tumor antigen sensitivity and persistence of CAR T cells targeting PSCA+ metastatic prostate cancer. Oncoimmunology 7, e1380764, doi:10.1080/2162402x.2017.1380764 (2018).

55. Crowe AR & Yue W. Semi-quantitative Determination of Protein Expression using Immunohistochemistry Staining and Analysis: An Integrated Protocol. Bio-protocol 9, doi:10.21769/BioProtoc.3465 (2019).
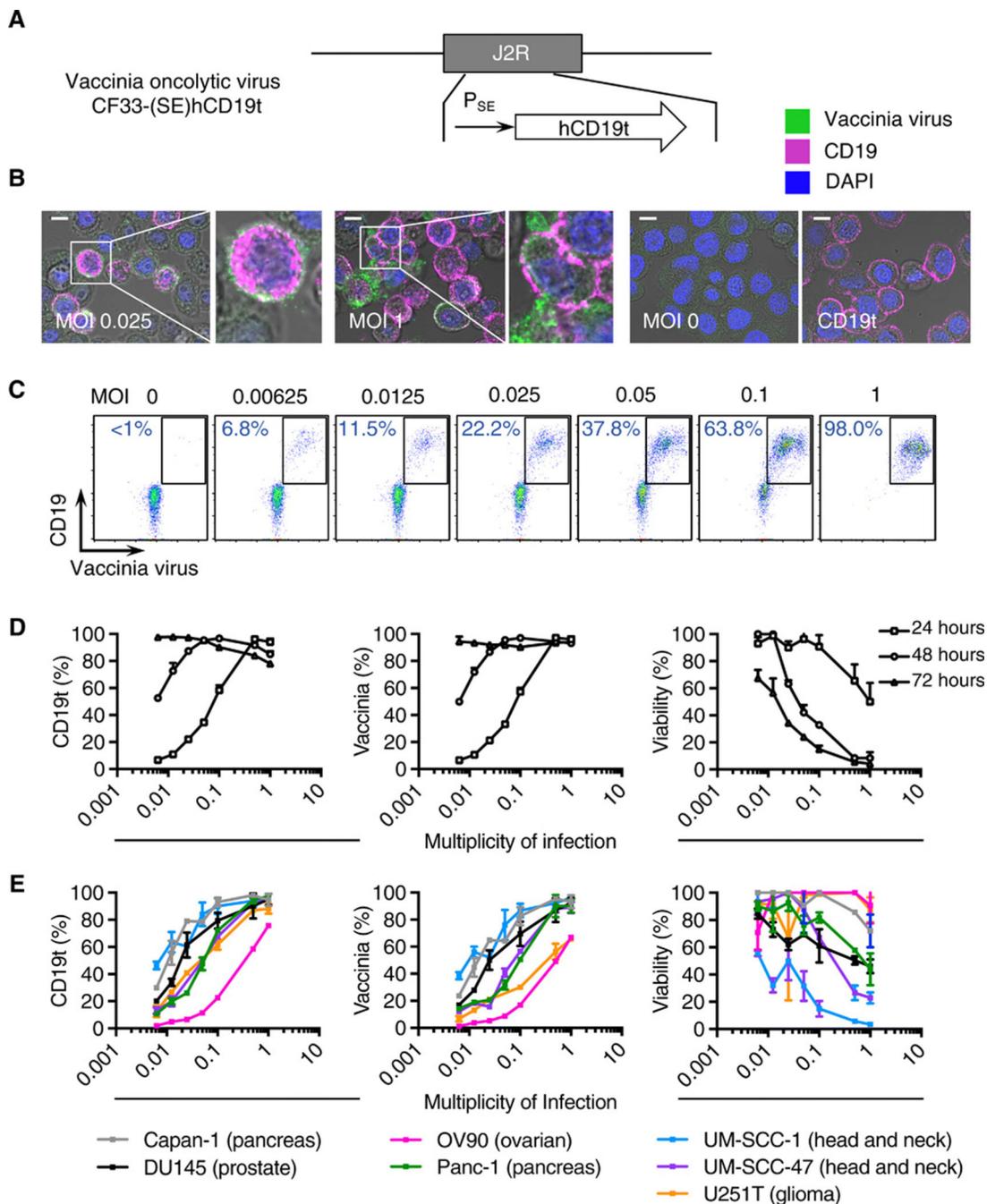
Fig. 1. OV effectively deliver CD19t to solid tumors in vitro.
(**A**) Schematic of vaccinia OV [CF33-(SE)hCD19t], showing incorporation of human truncated CD19 (CD19t) under the control of the synthetic early promoter (P_{SE}) inserted into the J2R locus and replacing the *thymidine kinase* gene. (**B**) Immunofluorescence microscopy of MDA-MB-468 cells infected for 24 h with OV19t at multiplicity of infection (MOI) 0.025 or MOI 1, untransduced (MOI 0), or cells transduced with lentivirus to stably express CD19t. Scale bars, 10 μm. Blue is DAPI, pink indicates CD19t, and green indicates vaccinia. (**C**) FACS plots of MDA-MB-468 tumor cells positive for CD19t and vaccinia

virus after 24 h of OV19t infection at increasing MOIs. Percents indicate CD19t-positive, virus-positive population in the boxed region. (**D**) Quantification of percent CD19t positive (left), vaccinia positive (middle), and viable (right) MDA-MB-468 tumor cells following 24, 48, and 72 h exposure to the indicated MOIs of OV19t. (**E**) Quantification of CD19t positive (left), vaccinia positive (middle), and viable (right) cells of indicated solid tumor cell lines following 24, 48, and 72 h exposure to the indicated MOIs of OV19t. Data in B and C are from one of at least two independent experiments. Data in D and E are presented as mean + SD (D) or mean ± SD (E) (n 2) from one of at least three independent experiments.
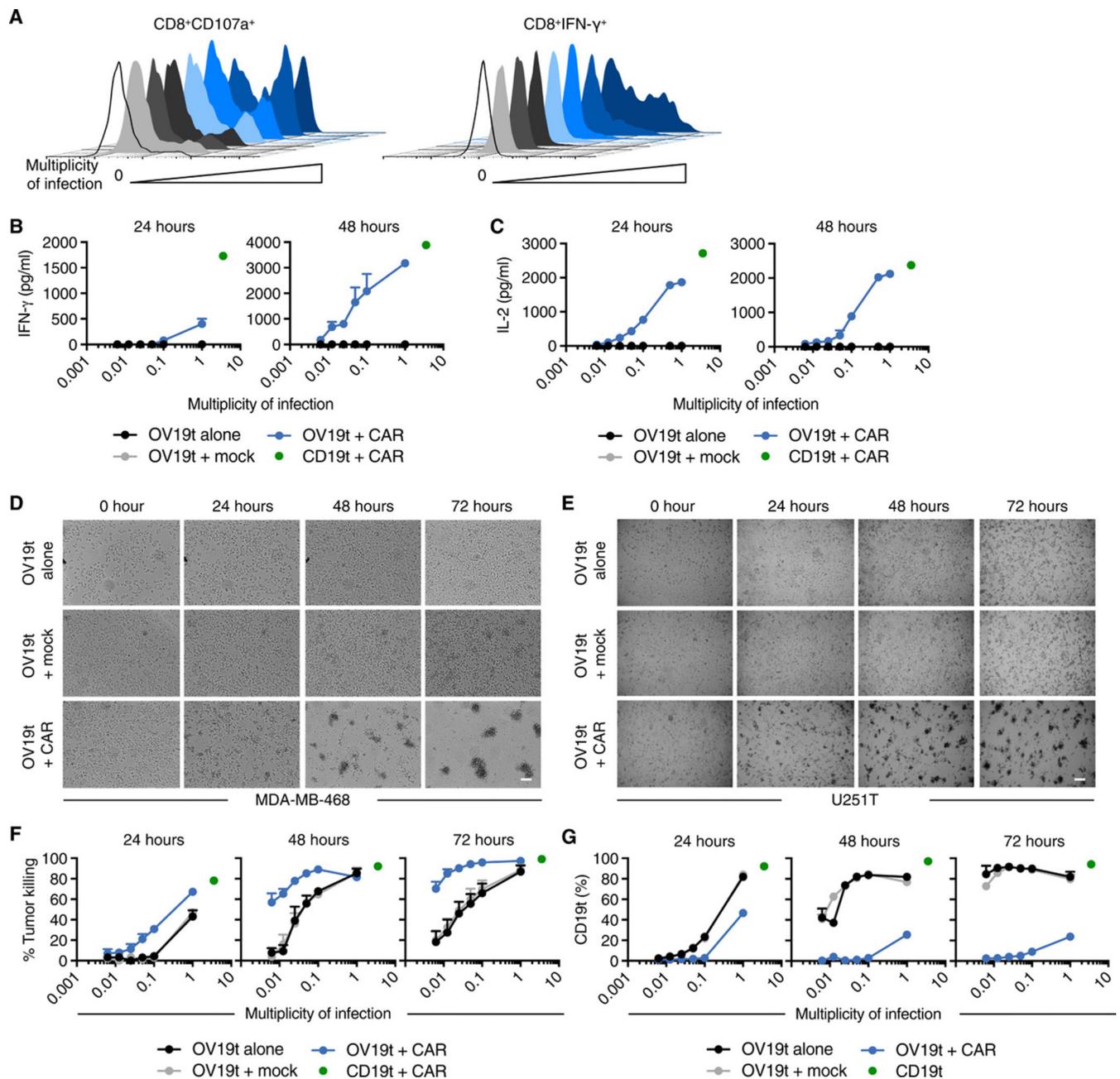
Fig. 2. OV19t introduces CD19t on tumor cells, which directs activation and cytotoxicity of CD19-CAR T cells in vitro.

(A) Representative flow cytometric analysis showing abundance of cell surface CD107a on and intracellular IFNγ in CD8$^+$CAR$^+$ T cells following 16-h coculture with MDA-MB-468 tumor cells in the presence or absence of the indicated MOI of OV19t. Ratio of effector CD19-CAR T cell to tumor cell was 1:1. Data are from one of two independent experiments. (**B**) IFNγ and (**C**) IL-2 production measured by ELISA in supernatants collected from cocultures in the presence or absence of OV19t at indicated MOIs for 24 and 48 h. Values for MDA-MB-468 cells stably expressing CD19t cocultured with CD19-CAR T cells (CD19t + CAR, green dot) are indicated by a single data point on each graph. Data

presented are from technical duplicates and shown as mean + SD. (**D, E**) Tumor killing assay of MDA-MB-468 (**D**) and U251T (**E**) cells visualized by phase-contrast microscopy. Representative images are shown. Scale bars, 200 μm. (**F**) Quantification of MDA-MB-468 cell killing assessed by flow cytometry. MDA-MB-468 tumor cells were cocultured with untransduced T cells (Mock) or CD19-CAR T cells for 24, 48, or 72 h in the presence of the indicated MOIs of OV19t. Values for MDA-MB-468 cells stably expressing CD19t cocultured with CD19-CAR T cells (CD19t +CAR, green dot) are indicated by a single data point on each graph. Data presented are from duplicate wells from two experiments and shown as mean + SEM. (**G**) Percent of MDA-MB-468 cells positive for CD19t in killing assay described in F. Values for MDA-MB-468 cells stably expressing CD19t cultured without CD19-CAR T cells (CD19t, green dot) are indicated by a single data point on each graph. Data presented are from duplicate wells and shown as mean + SEM.
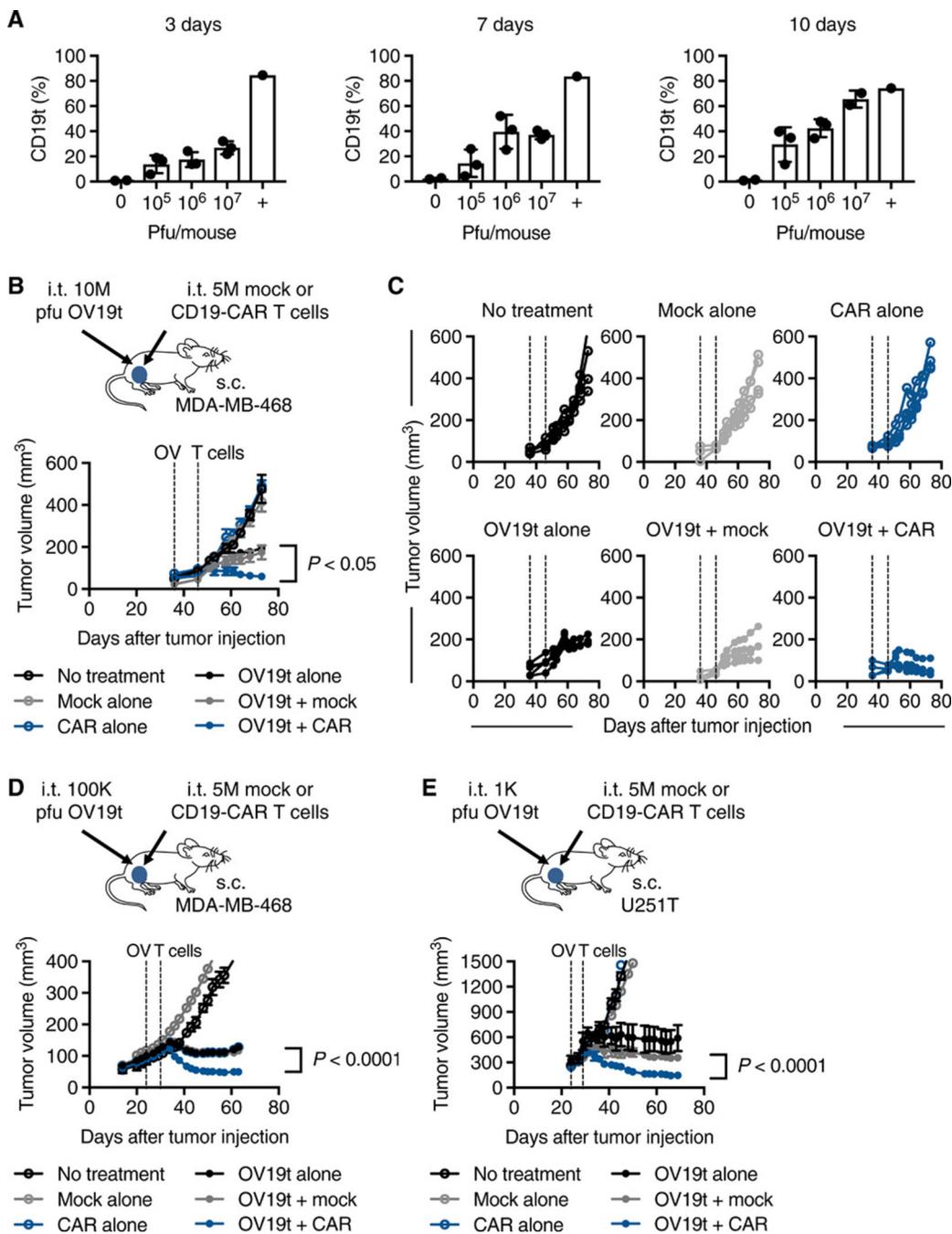
Fig. 3. Anti-tumor efficacy of combination therapy of OV19t and CD19-CAR T cells in human xenograft tumor models.
(**A**) Percent of CD19t-positive tumors cells. Mice were engrafted with subcutaneous MDA-MB-468 tumors (5×10^6 cells) and at day 24, mice were intratumorally injected with 0 ($n = 2$), 10^5, 10^6, or 10^7 ($n = 3$) plaque-forming units (pfu) of OV19t per mouse, which were harvested at day 3, 7, or 10 after treatment with OV19t. Percent cells positive for CD19t was quantified by flow cytometry. The positive control (+) represents MDA-MB-468 tumors stably expressing CD19t through lentiviral-mediated transduction prior to engraftment. (**B**)

Top: Schematic of MDA-MB-468 tumor-bearing mice treated with OV19t and CD19-CAR T cells. NSG mice were injected subcutaneously with MDA-MB-468 (5×10^6 cells) on day 0, and tumors were injected with OV19t (10^7 pfu, 10M) on day 36. On day 46, tumors were injected with either untransduced T cells (Mock) or CD19-CAR T cells (CAR, 5×10^6 cells). Bottom: Tumor volumes are shown as mean ± SEM (n 4 per group). (**C**) Tumor volumes for each mouse in each treatment group are shown for mice described in B. Dashed lines indicate OV and T cell injections. All data above are representative of two independent experiments. (**D**) Top: Schematic of MDA-MB-468 tumor-bearing mice treated with OV19t and CD19-CAR T cells. Experimental paradigm is the same as in B except tumor-bearing mice received intratumoral injections of OV19t (10^5 pfu, 100K) on day 24 and of either Mock T cells or CD19-CAR T cells (5×10^6 cells) on day 32. Bottom: Tumor volumes are shown as mean ± SEM (n 4 per group). (**E**) Top: Schematic of U251T tumor-bearing mice treated with OV19t and CD19-CAR T cells (top). NSG mice were injected subcutaneously with U251T (5×10^6 cells) tumors on day 0, and tumors were injected with OV19t (10^3 pfu, 1K) on day 24. On day 29, tumors were injected with either Mock or CD19-CAR T cells (5×10^6 cells). Bottom: Tumor volumes are shown as mean ± SEM (n 3 per group). P values indicate differences between OV19t + Mock and OV19t + CAR and were determined by unpaired Student's t test. s.c., subcutaneous; i. t., intratumoral.
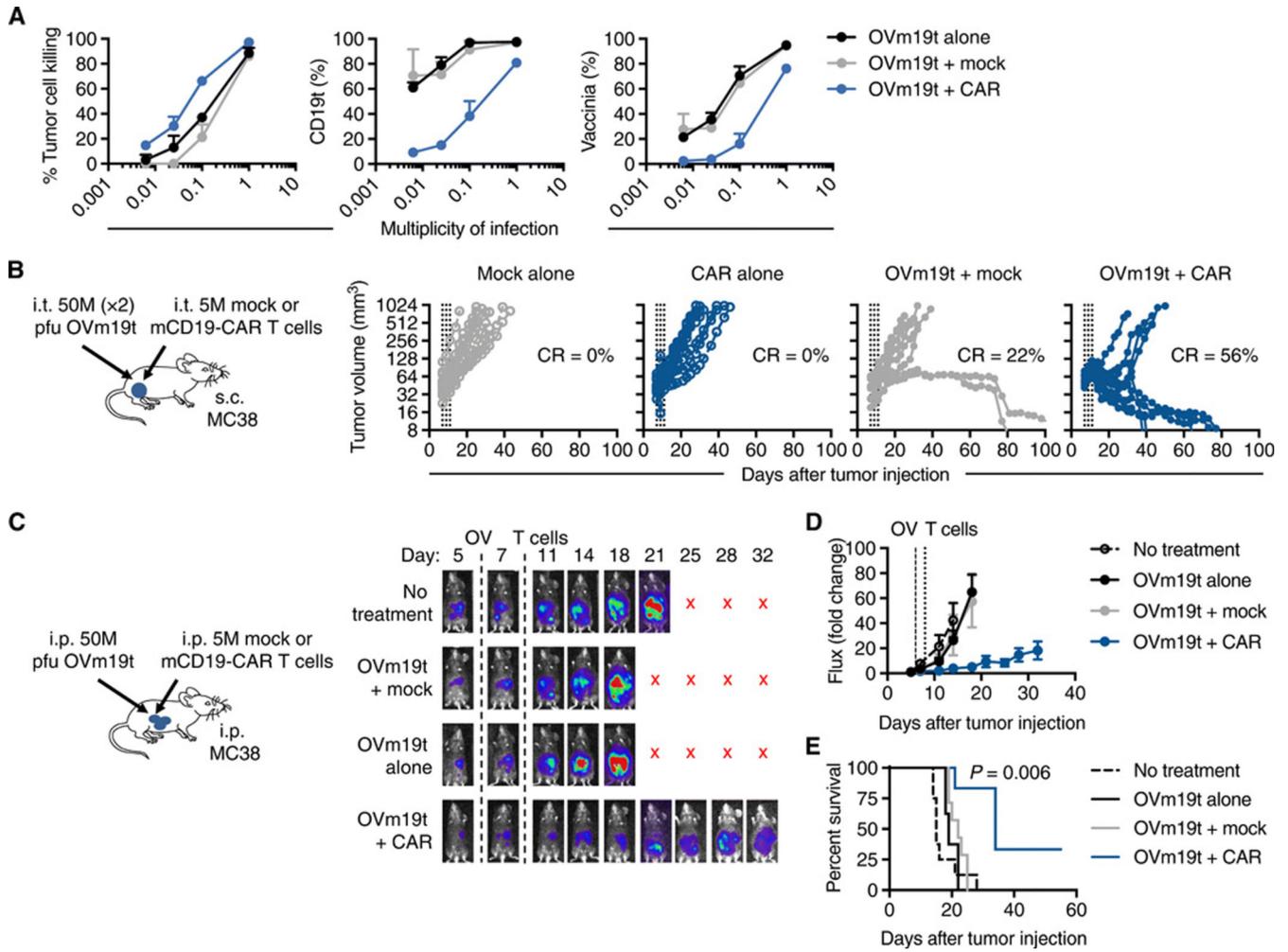
Fig. 4. Anti-tumor efficacy of combination therapy of OVm19t and mCD19-CAR T cells in an immunocompetent murine syngeneic tumor model.

(**A**) Tumor killing of MC38 tumor cells treated with the indicated MOIs of OVm19t and cocultured with mCD19-CAR T cells or untransduced T cells (Mock) for 24 h. Left: Tumor cell killing was assessed by flow cytometry. Middle: Quantification of percent tumor cells positive for CD19t. Right: Quantification of percent cells positive for vaccinia. (**B**) Left: Schematic of C57BL/6j mice with subcutaneous MC38 tumors treated with OVm19t and mCD19-CAR T cells. Mice were subcutaneously (s.c.) injected with MC38 cells (5×10^5 cells) on day 0. On days 7 and 9, mice were intratumorally treated (i. t.) with 0 or two doses of 5×10^7 pfu OVm19t per mouse. On day 11, mice were treated by intratumoral injection with either Mock or mCD19-CAR T cells (5×10^6 cells). Tumor volume was measured with calipers. Data for each mouse (n = 9 per group) is shown. Data are from one of two independent experiments. Percent of mice with complete response (curative response) is indicated. (**C**) Left: Schematic of C57BL/6j mice with intraperitoneal MC38 tumors treated with OVm19t and mCD19-CAR T cells. Mice were injected intraperitoneally (i.p.) MC38 cells expressing firefly luciferase (5×10^5 cells) on day 0. At day 6, mice were i.p. sham injected or were injected with 10^7 pfu OVm19t per mouse. On day 8, mice were i.p. injected with either Mock T cells or mCD19-CAR murine T cells (5×10^6 cells). n ≥ 6 per group.

Right: Tumor growth was measured by non-invasive optical imaging. X indicates mice were euthanized or had died. (**D**) Average tumor sizes (based on non-invasive imaging) are shown as mean ± SEM. (**E**) Kaplan-Meier survival curves from the experiment described in C. P value indicates difference between Ovm19t + Mock and OVm19t + CAR as determined by log-rank (Mantel-Cox) test.
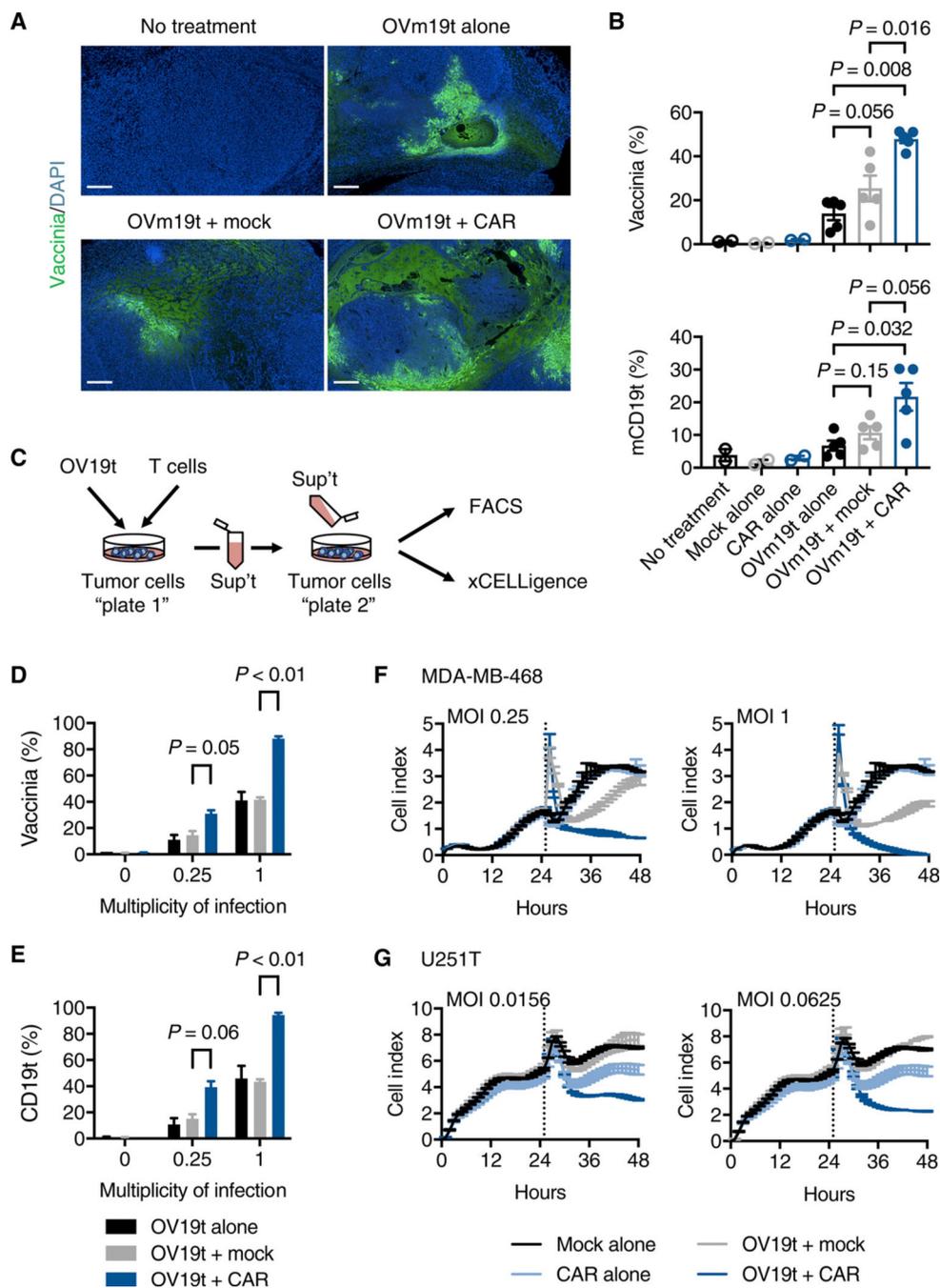
Fig. 5. CD19-CAR T cell-mediated tumor killing promotes the viral particle release and infection of tumor cells.

(**A**) Histology showing vaccinia virus in MC38 tumors harvested from mice with no treatment or treatment with OVm19t alone, OVm19t + Mock T cells, and OVm19t + mCD19-CAR T cells. T cell treatment was 2 days after OVm19t injection. Tumors were harvested and stained for vaccinia virus (green) 4 days after OVm19t alone or 2 days after T cell treatments. Scale bars, 500 μm. (**B**) Quantification of percent cells positive for vaccinia and mCD19t in subcutaneous tumors from mice receiving the indicated treatments. Mice

were injected subcutaneously MC38 tumors (5×10^5 cells) on day 0. On days 14 and 16 mice were intratumorally injected with OVm19t (5×10^7) pfu per mouse. On day 18 mice were treated intravenously with Mock T cells or mCD19-CAR T cells. Tumors were harvested 5 days after OVm19t or 3 days after T cell treatments. Cells were analyzed by flow cytometry. n = 2 – 5 per group. Statistical analysis using unpaired Student's *t*-test. (**C**) Schematic of experiment assessing viral release from MDA-MB-468 or U251T cells exposed to OV19t and Mock T cells or CD19-CAR T cells. In Plate 1, OV19t at varying MOIs were added to tumor cells for an initial 3 h incubation. Virus was washed off, and cells were incubated for an additional 4 h prior to adding Mock T cells or CD19-CAR T cells for 18 h. Supernatants were collected and added to freshly plated tumor cells (Plate 2) and incubated for 18 h. (**D, E**) Percent of cells positive for vaccinia (**D**) and CD19 (**E**) from Plate 2 was determined by flow cytometry. Data are shown as mean ± SEM from one experiment. Statistical analysis using unpaired Student's *t*-test. (**F, G**) Viable cells in Plate 2 receiving supernatants from Plate 1 cells exposed to the indicated MOI of OV19t. MDA-MB-468 (**F**) or U251T (**G**) cells were cultured for 24 h and then medium was replaced (dotted line) with supernatant from Plate 1 cells exposed to the indicated conditions. Viable cells were calculated as "cell index" using the xCELLigence RTCA system. Data are shown as mean ± SEM from one of two independent experiments.
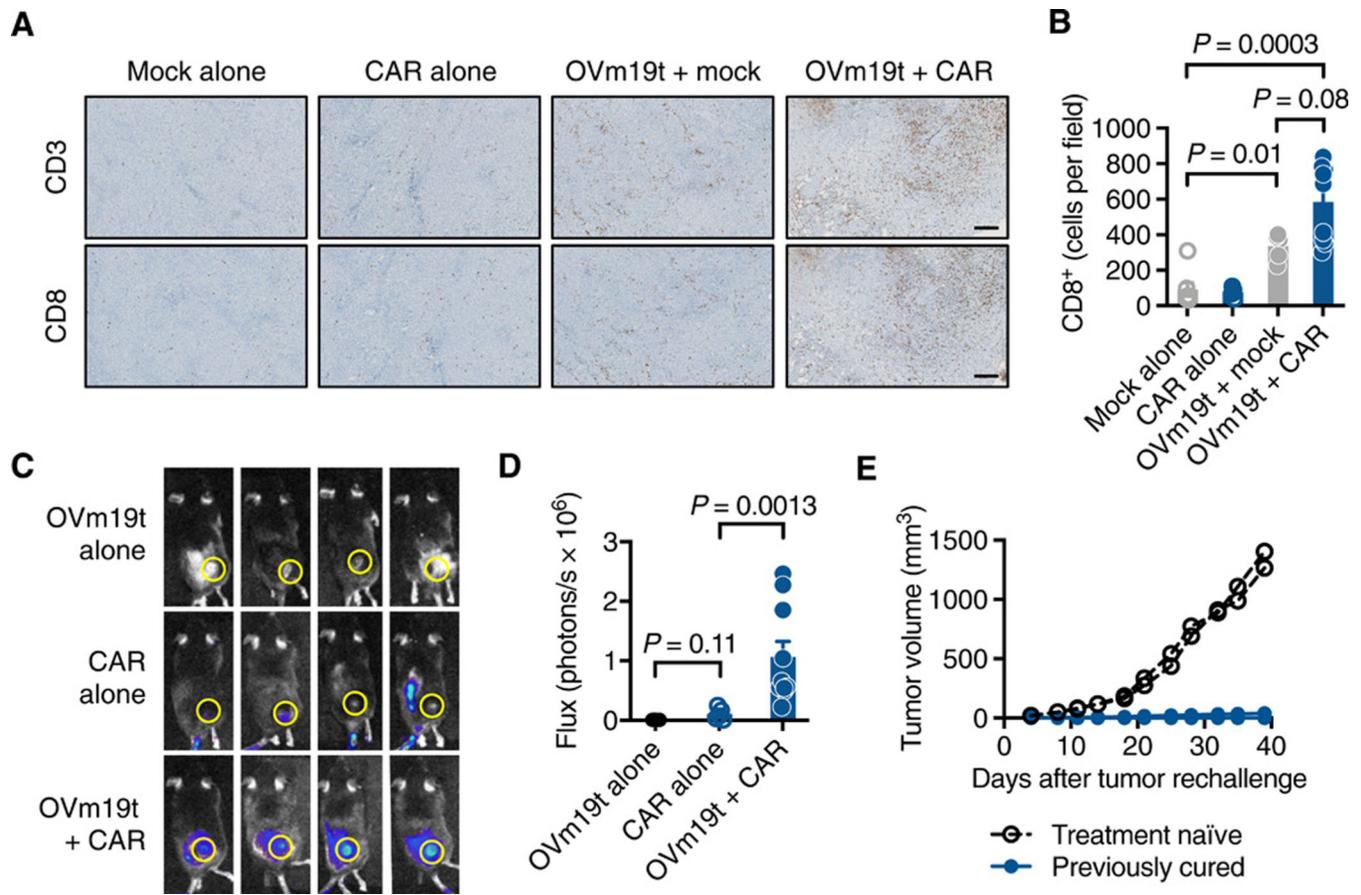
Fig. 6. OVm19t promotes tumor infiltration of both endogenous T cells and adoptively-transferred mCD19-CAR T cells.

(**A**) Histology showing murine CD3+ and CD8+ T cells in subcutaneous MC38 tumors harvested from mice treated intravenously with untransduced T cells (Mock) alone, mCD19-CAR T cells alone, OVm19t + Mock T cells, and OVm19t + mCD19-CAR T cells. Tumors were harvested 4 days after T cell administration and 6 days after OVm19t injection. Scale bars, 250 μm. (**B**) Quantification of immunohistochemical staining for murine CD8+ cells in tumors from mice treated as in A. Symbols indicate individual tumors from mice. Statistical analysis using unpaired Student's *t*-test. (**C**) Representative flux imaging of mice 2 days after treatment with intratumoral OVm19t alone (n = 4), intravenous firefly luciferase-expressing mCD19-CAR T cells alone (n = 5), or OVm19t + firefly luciferase-expressing mCD19-CAR T cells (n = 10). (**D**) Quantification of T cell flux from the regions of interest shown in C. Symbols indicate flux for each mouse. Statistical analysis using unpaired Student's *t*-test. (**E**) Tumor volume in treatment-naïve or previously cured C57BL/6j mice rechallenged by subcutaneous injection of MC38 (5×10^5) cells. n = 7 for rechallenge group, n = 2 for treatment-naïve group. Individual tumors from mice are shown.